Wear 595 (2026) 206691

Contents lists available at ScienceDirect

Wear

journal homepage: www.elsevier.com/locate/wear

Reciprocating sliding wear performance of cold spray additive manufactured titanium

Paloma Sirvent [a,*], Xavier Soldani [b], Miguel Ángel Garrido-Maneiro [a], Pedro Poza [a,c]

[a] DIMME – Durability and Mechanical Integrity of Structural Materials, Escuela Superior de Ciencias Experimentales y Tecnología, Universidad Rey Juan Carlos, C/ Tulipán s/n, Móstoles, 28933, Madrid, Spain
[b] Mechanical Engineering Department, Universidad Pontificia Comillas, Alberto Aguilera 25, 28015, Madrid, Spain
[c] Instituto de Tecnologías para la Sostenibilidad. Universidad Rey Juan Carlos, Spain

ARTICLE INFO

Keywords:
Cold spray additive manufacturing
Titanium
Micro-scratch wear
Reciprocating sliding wear

ABSTRACT

Titanium's extensive use in several applications, such as in aeronautical or automotive parts or biomedical implants, necessitates the development of Ti components in diverse shapes and sizes. Moreover, these components are usually subjected to mechanical wear, as that generated in the contact between materials subjected to a back-and-forth relative motion. Therefore, this study investigates the applicability of Cold Spray Additive Manufacturing (CSAM) for producing pure Ti components, focusing on their tribological properties under reciprocating sliding conditions. Two CSAM Ti samples sets, fabricated with different process parameters (55 bar and 800 °C for Ti-55-800, and 60 bar and 1000 °C for Ti-60-1000), were evaluated. Microstructural analysis by optical and scanning electron microscopy showed that the Ti-60-1000 sample had approximately 30 % lower porosity than the Ti-55-800 sample, as well as larger bonding areas between splats. Mechanical testing, including hardness and elastic modulus measurements via nanoindentation, and tribological analysis showed similar wear behavior at the local scale, with the Ti-60-1000 sample exhibiting higher hardness (2.37 GPa). Wear behavior was assessed at the microscale through scratch tests, and at the macroscale using pin-on-disc tests under reciprocating sliding conditions. The Ti-60-1000 sample presented a higher macroscopic wear resistance due to the enhanced bonding between splats observed in its microstructure. The study highlights the importance of reducing porosity and increasing bonded areas in CSAM Ti samples to enhance their mechanical and tribological properties. These findings suggest that CSAM technology holds promise for manufacturing Ti parts for different applications, offering environmental and economic benefits.

1. Introduction

The extensive use of titanium (Ti) in numerous applications necessitates the development of Ti components in various shapes and sizes while displaying the required properties. To address a wide range of high value-added applications, such as those found in the aerospace industry, it is essential to rely on a manufacturing technique capable of adapting to demanding requirements in both geometry and performance, while ensuring minimal material waste. In this context, additive manufacturing, or 3D printing, emerges as a highly advantageous option [1].

Additive manufacturing (3D printing) of aerospace alloys offers substantial advantages, enabling the production of lightweight, topologically optimized structures that significantly reduce component mass while maintaining high mechanical performance. The process allows the fabrication of geometries that are impossible or highly inefficient to achieve through conventional machining, such as internal cooling channels, lattice architectures, and consolidated multi-function components. For high-value materials like Ti-6Al-4V, 3D printing dramatically lowers the buy-to-fly ratio by minimizing waste, making the process both cost-effective and sustainable. Rapid solidification during printing often results in refined microstructures that meet or exceed the strength and fatigue properties of forged alloys, especially after appropriate heat treatments. Additionally, additive manufacturing shortens lead times, reduces the need for tooling, and supports on-demand production of complex aerospace components, offering major

* Corresponding author.
E-mail addresses: paloma.sirvent@urjc.es (P. Sirvent), xsoldani@comillas.edu (X. Soldani), miguelangel.garrido@urjc.es (M.Á. Garrido-Maneiro), pedro.poza@urjc.es (P. Poza).

https://doi.org/10.1016/j.wear.2026.206691
Received 15 September 2025; Received in revised form 27 March 2026; Accepted 28 March 2026
Available online 29 March 2026

benefits for prototyping, customization, and maintenance operations [2], [3]. Consequently, the development of Ti products through additive manufacturing is of particular interest. To mention a few examples, this material is used for landing gear parts in aeronautics, for automotive engine parts, or for medical implants, where complex forms are required [4], [5]. Most of these components are deteriorated by wear, as that arising at the contact between two components which are subjected to a cyclic back-and-forth relative motion.

The material processing technique significantly influences the final properties of the material and its sustainability, which is especially relevant for light metal components due to their high processing costs and scarcity [6], [7]. Several studies have already reported the successful deposition of titanium, titanium alloys and titanium compounds using different thermal spray and additive manufacturing techniques such as plasma spraying, high-velocity oxy-fuel (HVOF) or flame spray [8], [9]. However, as a light metal alloy, Ti exhibits high reactivity, posing challenges for processing techniques that involve high-temperature procedures. In this context, Cold Spray (CS) technology is highlighted for its use of low processing temperatures during spraying, which means that the feedstock powder is sprayed in a solid or semisolid state [10]. In recent years, researchers have shown increased interest in this technology, initially for repair purposes and more recently for additive manufacturing of Ti components [11], [12]. The advantages of this technology stem from the fact that particles are sprayed in a solid or semi-solid state [10]. This allows the coating to preserve the chemical and structural phases of the feedstock material, preventing oxidation. Additionally, the absence of a melting process and subsequent solidification avoids the generation of residual stresses in the coating, enabling the creation of thicker coatings compared to other thermal spray techniques. Consequently, this technology is now being studied for additive manufacturing. Furthermore, CS coatings can enhance the mechanical properties of the material due to the cold work hardening effect from the plastic deformation of the particles.

Recent studies show that CSAM pure Ti samples present similar features as those of the CS pure Ti samples from the microstructural and mechanical points of view [13], [14]. CS pure Ti coatings have been extensively investigated from microstructural [15], [16] and mechanical perspectives [17], [18]. These works reveal that Ti bonding mechanisms have unique characteristics compared to other materials due to Ti's lower plastic deformation capacity compared to metals like Cu or Al. Consequently, the CS process requires significantly higher kinetic energy to ensure particle cohesion. Dense coatings have been achieved using higher particle velocities [16], [17], and employing a light gas like He and N_2 with process gas temperatures over 800 °C and pressures over 4 MPa. Despite challenges in obtaining dense Ti materials by CSAM, this technique offers mechanical behavior advantages. Hardness studies of Ti CS samples show increased hardness compared to bulk or feedstock material [13], [17], [18], with hardness values ranging from 2 to 3 GPa for CS pure Ti samples, slightly above bulk Ti values of 1.5 to 2 GPa [19], [20].

To evaluate a material for a particular application in which mechanical wear occurs it is necessary to study the wear behavior through a representative wear configuration similar to the actual wear system. Abrasive wear is one of the most widespread and technically relevant wear processes, making abrasive wear resistance a key performance indicator in industrial materials subjected to sliding or particulate contact. Abrasive wear is a critical degradation mechanism in titanium alloys used in aerospace structures, where components are routinely exposed to particulate matter, fretting interfaces, and harsh operating environments. The combination of relatively low hardness and high reactivity in Ti-based alloys, such as Ti-6Al-4V, can exacerbate material loss under abrasive conditions, directly affecting dimensional stability, surface integrity, and service life. Given that wear-induced damage can compromise structural reliability, increase maintenance demands, and limit component longevity in demanding aeronautical settings, evaluating abrasive wear resistance becomes essential [21]. For this reason, wear has been evaluated in CS pure Ti samples under different abrasive conditions. Most tribological characterizations of Ti CS samples until the date involve ball-on-flat tests to evaluate Ti wear behavior for general engineering applications [22], [23]. Investigated motions include linear reciprocating [23] and rotational [22]. Linear reciprocating studies were performed with 6 mm diameter balls made of various materials (alumina, steel, and silicon nitride), with linear velocities ranging from 1 mm/s to 20 mm/s and loads between 0.5 and 9 N. The wear rates were in the order of 10^{-4} to 10^{-5} mm^3/Nm. Conversely, rotational wear tests used a steel ball, with wear rates in the order of 10^{-4} mm^3/Nm [22]. Additionally, only one paper reports micro-scratch test analyses on CS pure Ti coatings [24], investigating wear behavior through scratch tests on low porosity (<2 %) CS Ti coatings. This study reveals effects such as microfractures and particle decohesion caused by the scratch action, but no quantitative wear rates are provided. However, the tribological characterization of CS or CSAM pure Ti coatings has been scarcely investigated, making current studies insufficient to determine the applicability of CSAM samples. Particularly, to the authors' knowledge, there are no studies related to wear under back-and-forth sliding conditions. It is worth noting that wear analyses of Ti alloys, like Ti6Al4V, showed higher wear rates in reciprocating conditions compared to continuous conditions [25]. This particular sliding mode is found, for example, between the elements of wing flap mechanisms or landing gears retrieving mechanisms of an airplane [26], as well as on hip implants in the field of biomedicine [27]. These wear systems are generally lubricated in service, and thus, the lubrication should be considered in the experimental evaluation of the wear behavior. However, preliminary investigations are often conducted without lubrication in order to explore the behavior of the materials and the wear mechanism [28], [29]. The unlubricated studies are important in order to identify features to first minimize wear in dry conditions. In this step, the material wear response can be improved, for example, by modifying the processing parameters of the sample fabrication procedure or performing a surface treatment. However, before moving in that direction, it is necessary to first investigate how CSAM-fabricated Ti components behave under standard processing conditions when subjected to reciprocating wear. This step is essential to determine whether CSAM can produce titanium parts with adequate tribological performance. The present study therefore provides a foundational assessment that can serve as a basis for future work aimed at producing components using optimized spraying parameters to further improve their tribological performance.

For this reason, the aim of this work is to evaluate the tribological properties under reciprocating sliding conditions of CSAM pure Ti samples. Two CSAM samples sets fabricated with different process gas temperatures and pressures were evaluated. The microstructure of the samples was analyzed, followed by hardness and elastic modulus measurements via nanoindentation. Wear behavior was first analyzed at microscale through scratch tests and then, macroscale wear tests were performed by pin-on-disc tests under bidirectional sliding conditions. The results are discussed to evaluate the potential application of Ti CSAM samples for components subjected to back-and-forth sliding wear. Additionally, the study provides insights into CSed materials characterization by distinguishing properties at the macroscopic scale, considering the entire deposited material, affected by inherent defects, from those at the microscopic scale unaffected by defects like porosity. Evaluating properties at microscale is particularly important for optimizing CSAM samples.

2. Materials and methods

2.1. Cold spray samples deposition

Two different CSAM Ti samples sets were studied in this work, each fabricated under distinct spraying conditions. Fabrication was carried out using a Plasma Giken PCS100 cold spray system at the Thermal Spray Centre (CPT, Barcelona, Spain). The feedstock material used for

spraying was pure Ti (grade 2) powder provided by AP&C (Boisbriand, QC, Canada). Moreover, the CSAM samples were built up on commercial Ti6Al4V plates, which were previously treated by grit-blasting. Spraying was performed with nitrogen as process gas, maintaining a stand-off distance of 40 mm and a 90° angle relative to the substrate. The traverse speed was set at 500 mm/s, with a track spacing of 1 mm. The cold spray parameters varied for each studied sample set were the process gas pressure and temperature. They were defined at 55 bar and 800 °C for the first sample set, and 60 bar and 1000 °C for the second one. In this work, these samples sets will be named as Ti-55-800 and Ti-60-1000, respectively.

The selection of these spraying conditions is based on literature. Previous studies have already reported the CS parameters that give rise to dense pure Ti samples using nitrogen as process gas. The first studies in literature demonstrating dense CS pure Ti samples showed that such compact deposits could be achieved using nitrogen as the process gas working at around 800 °C and 40 MPa [17], [30]. The subsequent introduction of next-generation cold spray systems, capable of operating at higher temperatures and pressures, has since enabled the reliable production of dense Ti deposits under higher values of the process gas conditions, with the upper limits explored reaching 900-1000 °C and 60 MPa [31], [32]. Within this expanded processing envelope, the two selected parameter sets in the present work are justified as follows: the first establishes a moderate temperature known to be effective for Ti, and the second represents the practical maximum for spraying pure Ti powder.

2.2. Microstructural characterization

X-ray diffraction (XRD) analyses were conducted on the powder and CSAM samples to characterize the structural phase composition. The experiments were conducted with a Philips PW3040/00 X'Pert MPD/MRD equipment. The diffraction patterns were recorded using an angle step of 0.02°, while the angle width varied from 15° to 100°. The peak identification was done using the PDF-5+/Web database (based on the International Centre Diffraction Data, ICDD).

The samples microstructure was examined to evaluate their quality. For this purpose, metallographic preparation was performed on cross-sectional cuts of the samples obtained from both parallel and perpendicular spraying directions. The typical three-step preparation procedure was followed to achieve a mirror-like surface: grinding with 320 grit SiC paper, polishing with 9 μm diamond paste, and final grinding with colloidal silica suspension (0.04 μm).

The samples were initially analyzed using optical microscopy to measure their thickness and porosity. A Motic BA310 Met-T optical microscope was employed for this purpose. Thickness was determined from the average values of at least 30 measurements taken along the sample's cross sections. The porous distribution was found to be inhomogeneous along the sample thickness, so porosity was calculated at three different zones: the first zone from the interface with the substrate up to 500 μm, the second one from 500 to 1500 μm, and the third from 1500 μm to the sample's surface. The porosity value in each zone was obtained as the average percentage porosity calculated from five different images (at 50× magnification) for each sample.

The samples were then examined using scanning electron microscopy (SEM) to evaluate the bonding between different splats, as well as between the splats and the substrate, and to analyze the splats' morphology. Additionally, the feedstock powder morphology and chemical composition were investigated using SEM. A Hitachi S3400N scanning electron microscope was used to acquire secondary electron (SE) and backscattered electron (BSE) images. Furthermore, energy dispersive X-ray microanalysis (EDX) was employed to characterize the chemical composition, using a Bruker XFlash 5010 EDX detector attached to the microscope. For the SEM investigation, the samples were etched with Kroll's reagent.

2.3. Mechanical properties

Nanoindentation tests were performed on the feedstock powder and samples to measure hardness (H) and elastic modulus (E). The tests were conducted on the longitudinal and transverse samples sections and on the cross sections of the Ti particles used for spraying. The samples were metallographically prepared before testing. For this purpose, the samples were mounted in epoxy resin, while the powder was mounted in a Sn-Ag matrix to provide a relatively stiff matrix for the Ti particles. This latter mounting procedure has been previously reported [33], [34] as a method to increase the penetration depth range where valid E and H values can be obtained.

A matrix of 30 indents was performed on the samples to obtain the average and standard deviation values of the calculated mechanical properties in the tests. The data analysis to obtain hardness and elastic modulus was conducted following the Oliver and Pharr methodology [35], and tip calibration was performed on a Ti6Al4V alloy (E = 110 GPa). The indentations were conducted using the continuous stiffness measurement (CSM) technique. The CSM consists of superimposing a dynamic oscillation of continuous loading and unloading cycles to the loading movement applied to the indenter. From these measurements, it is possible to obtain the contact stiffness from the slope of the initial unloading curves in each cycle. Therefore, this allows to determine the evolution of the mechanical properties as a function of the indenter penetration depth. In this work, the maximum indentation depth was set at 2000 nm for the CSAM samples and 300 nm for the powder particles, and the oscillations were done with an amplitude of 2 nm and a frequency of 35 Hz.

The harmonic contact stiffness vs. indentation depth curves were examined beforehand to discard data ranges affected by factors such as a low stiffness mounting medium (for the powder) or porosity (for the samples) [33]. The criteria for selecting the valid data range for calculating the elastic modulus and hardness were based on the linear correlation of harmonic contact stiffness with indentation depth [36], as illustrated in Fig. 1a. This figure shows a representative example of the obtained harmonic contact stiffness curves indicating how in this test the valid data range for the mechanical properties analyses was up to 500 nm of penetration depth.

Conversely, Fig. 1b presents the evolution of hardness as a function of penetration depth for a test conducted on one of the samples as a representative example. This graph shows that the available data range for the analysis was affected by the indentation size effect [37], that is, the hardness variation with the applied load. It can be seen in the figure that the validated data range for the mechanical properties analyses was entirely affected by this effect, and thus the hardness did not reach an asymptotic value. The asymptotic hardness was therefore evaluated using the Nix and Gao model [37] as shown in Fig. 1b.

2.4. Scratch resistance

Scratch tests were conducted to characterize the abrasive wear caused by hard particles on the materials under study. The scratches were made at the nanoscale using the same nanoindenter as for the nanoindentation tests, with the same Berkovich indenter oriented face-forward during the tests.

The tests were performed on the samples' cross sections, which were previously metallographically polished. Scratches were made over a length of 200 μm, applying a constant normal load (F_n) of 30 mN and a speed of 10 μm/s. Six test replicas were conducted on each sample. The data collected from each scratch test included the longitudinal profile and the coefficient of friction (COF). Additionally, the transverse topography of the residual groove was measured through three cross profiles, spaced 25 μm.

To calculate the wear rate, the residual groove volume per unit distance was estimated using a confocal microscope (Lambda-2, Rtec Instruments) and a data analysis software (Gwyddion). Regions without

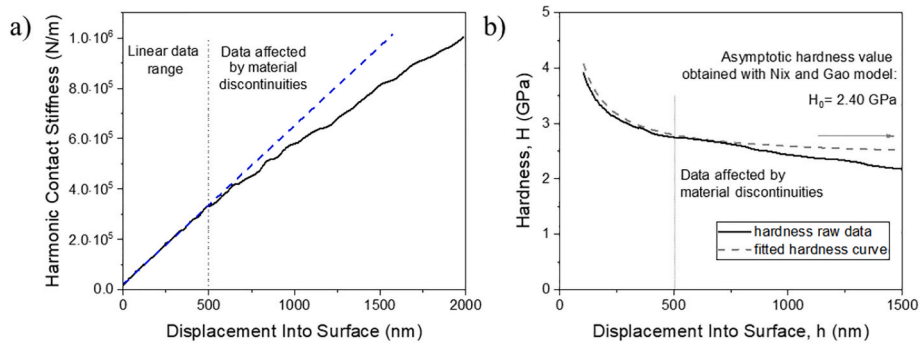

Fig. 1. a) Harmonic contact stiffness and b) hardness evolution with the indentation depth obtained from an indentation performed on the Ti-60-1000 sample. The asymptotic hardness estimated using Nix and Gao model has been also included.

pores were selected from the entire 3D image of the groove, as shown in Fig. 2, to calculate the volume. First, median leveling was applied to the surrounding surface of the groove to set the reference plane. Then, the displaced wear volume was estimated by applying a mask with a threshold to select the data from the surface plane (reference plane) to the deepest point in the groove. Conversely, the pile-up volume was estimated by applying an inverted mask, from the surface plane to the highest point in the pile-up. Both the displaced wear volume and the pile-up volume were expressed per unit distance using the corresponding length measurement in each groove section. The results report the average and standard error of at least five measurements from different groove sections for each material.

Finally, to characterize the wear resistance to scratching, a specific wear rate, k_s, was calculated using the Archard equation [38]. This constant represents the ratio of the removed material volume by sliding distance (w) by the applied normal load (F_n), expressed in units of mm^3/Nm.

2.5. Wear behavior under reciprocating conditions

The tribological tests at the macroscale were conducted under reciprocating sliding conditions using a pin-on-disc tribometer (Wazau TRM 1000). A schematic illustration of the pin-on-disc configuration performing a back-and-forth motion is shown in Fig. 3, which includes a transverse view and a plane view. The distance from the disc center to the pin position (R) was 26 mm. Pieces with a flat surface area of 2.5 × 5 mm^2 were prepared from the CSAM samples under study to serve as the pin, while the discs were fabricated from 100Cr6 steel ($R_a = 0.62 \pm 0.07$ µm, 760 ± 17 HV). The tested pieces correspond to different samples within the sprayed sets. The samples were cleaned and degreased before the tests, but the roughness was not modified; the surface roughness of

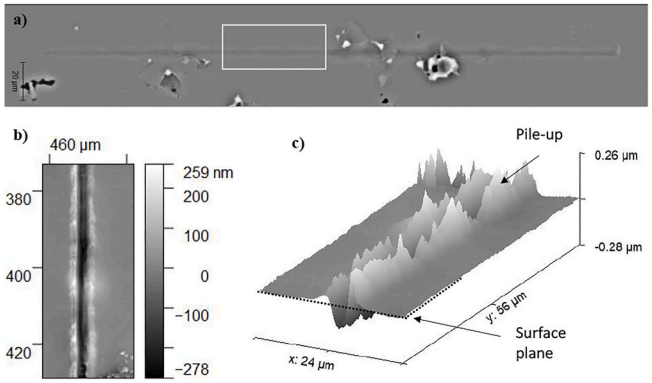

Fig. 2. a) 2D image of an entire wear scar of a scratch test performed on the Ti-60-1000 sample, b) a 2D image with height scale bar of the groove section without pores squared in (a) and (c) its corresponding 3D image.

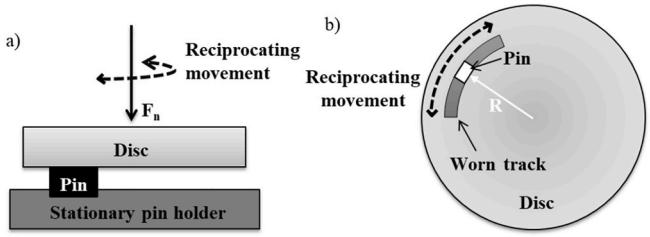

Fig. 3. Schematic representation of the a) transversal and b) plane view sections of the pin on disc configuration performance under reciprocating movement.

the CSAM samples generated during deposition was maintained. The roughness of both the CS samples and the discs was measured using the same confocal microscope employed for volume estimation in the scratch tests.

The wear behavior of the samples was investigated under three different sliding amplitudes while keeping all other test parameters constant. The tests were performed at room temperature and at a constant contact pressure of 6.6 MPa between the pin and the disc. In the present configuration, the reciprocating movement is performed along an arc length rather than along a linear length, as shown in Fig. 3b. The selected arc lengths in this study were set defining the following central angles: 30°, 60°, and 120°. With the frequency set constant at 0.9 Hz, the sliding velocities were 24.5, 49, and 98 mm/s, respectively for each angle. These testing conditions were selected to simulate a bidirectional movement for different applications. Additionally, a wear limit was established by setting a maximum wear depth of 1 mm, detected using a linear variable differential transformer sensor (LVDT). This condition determined the total number of cycles and, consequently, the total sliding distance of the wear test for each oscillation angle and for each material. Two replicas of each testing condition were conducted. In all the samples tested the results obtained were in a reasonable agreement.

The wear rates were calculated using the Archard equation for abrasive wear [39]. To estimate the wear volume, the weight loss of the pins was measured by weight difference, using a balance (Metler Toledo) with five decimal digits for precision. Conversely, the coefficient of friction (COF) was continuously recorded during the tests. The average COF value reported in the paper was calculated as the mean value of the data range where the COF stabilized.

3. Results and discussion

3.1. Microstructural characterization

Fig. 4a shows an image of the feedstock pure Ti powder. The particles were spherical in shape and exhibited varying sizes. The particle diameter size distribution, shown in Fig. 4b, indicates that the diameters

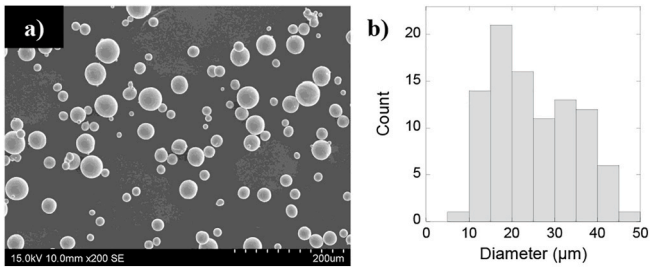

Fig. 4. a) SEM image showing the feedstock powder with spherical morphology, b) the particles size distribution in terms of the diameter.

ranged between 5 and 50 μm, with a mean value of 25 ± 9 μm.

The structural phase composition of the powder was characterized by XRD (Fig. 5). The diffraction pattern was indexed with the PDF card 01-086-2608, which corresponds to the α-Ti phase (hexagonal close-packed (hcp) structure, $P6_3/mmc$ space group, a = b = 2.951 Å and c = 4.681 Å). The 2θ positions of the three principal diffraction peaks of this phase are, in order of diffraction intensity magnitude: 40.16°, 38.43° and 35.08°.

Fig. 5 also reports the XRD patterns obtained from the CSAM sample surfaces. The diffraction peaks of the α-Ti phase were shown to be shifted 0.5° to the left for both studied samples, Ti-55-800 and Ti-60-1000. This peak shift is typically observed in CS samples, and it is related to the residual stresses generated during spraying [40].

The external appearance of the as-sprayed samples exhibited a wavy texture created by the CS deposition process, which involved spraying the powder in parallel lines. The texture was similar for both samples, as they presented comparable roughness values, as reported in Table 1.

Fig. 6 presents transverse cross-sections of the as-sprayed samples. The sample thicknesses were quite similar, with the Ti-60-1000 sample being 13 % thicker than the other. Additionally, the samples showed a non-homogeneous porosity distribution. The SEM images (Fig. 6) clearly show that the upper region of the samples exhibited a higher level of porosity, particularly in the Ti-55-800 sample. This variability was quantified by measuring the porosity in three different regions along the sample thickness, as shown in Fig. 7a. The zone next to the substrate represented the first 500 μm of sample height, the second zone consisted of the following 1000 μm, and the third zone included the remaining part from 1500 μm up to the sample's top surface. The porosity distribution followed a similar trend along the thickness of both samples (Fig. 7b). The first zone had similar porosity compared to the middle zone, while the porosity significantly increased in the upper region. Additionally, the Ti-55-800 sample exhibited higher porosity, ranging between 8.8 % and 19.9 %, compared to the Ti-60-1000 sample, which ranged between 5.8 % and 9.8 %. Thus, the porosity was reduced by up to about 30 % in zones 1 and 2 in the Ti-60-1000 sample.

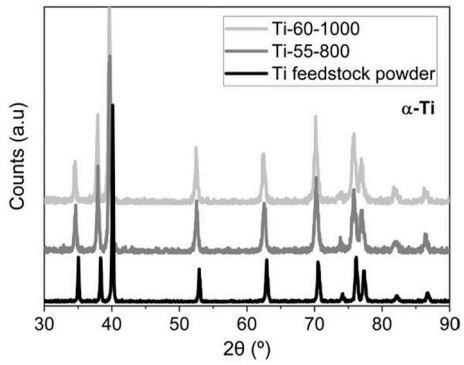

Fig. 5. XRD pattern of the powder and of the CSAM samples Ti-55-800 and Ti-60-1000.

Table 1
Arithmetic average roughness (R_a), root mean square average roughness (R_q) and maximum height profile (R_z) of the as-sprayed samples surface.

CS Sample	R_a (μm)	R_q (μm)	R_z (μm)
Ti-55-800	8.45 ± 0.48	10.43 ± 0.66	50.75 ± 3.53
Ti-60-1000	8.77 ± 0.95	11.06 ± 1.19	55.53 ± 6.80

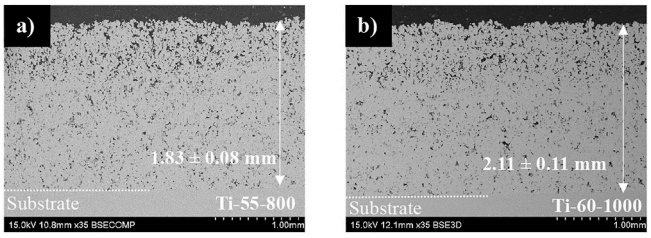

Fig. 6. BSE images of transversal cross-sections of the a) Ti-55-800, and b) Ti-60-1000 samples. The average thickness of the coatings is also included.

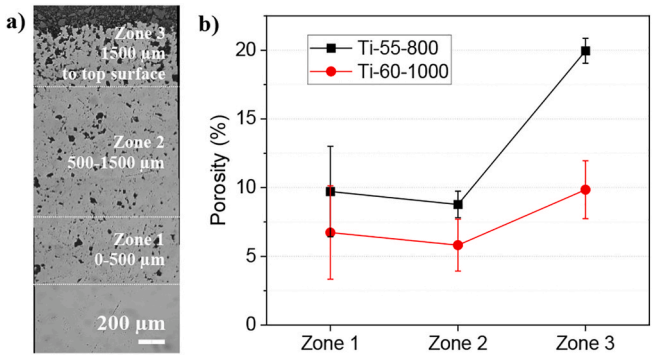

Fig. 7. a) OM micrograph of the Ti-60-1000 sample showing the sample transversal section partition in three zones to quantify the porosity distribution; and b)graphic representation of the porosity distribution along the three defined zones of the Ti-55-800 and Ti-60-1000 samples cross sections.

Fig. 8 shows cross-sectional images of the etched microstructure of the samples under study. The characteristic splat microstructure of cold-sprayed samples was observed. Additionally, a martensitic microstructure can be distinguished within the splats. Metallurgical bonding was generated between the splat interfaces, with some marked as dotted lines in Fig. 8. It was observed that the bonding areas along the interface of each individual splat were larger in the Ti-60-1000 sample, as seen in Fig. 8.

The microstructural analysis aligns with literature, as an increase in the process gas temperature and pressure is known to lead to denser coatings. This result has been demonstrated particularly for CS pure Ti in a work by Gulizia et al. [41], where they examined the microstructure of sprayed samples at process gas pressures ranging from 2 to 3.5 MPa and temperatures between 400 and 800 °C. The porosity analyses of those

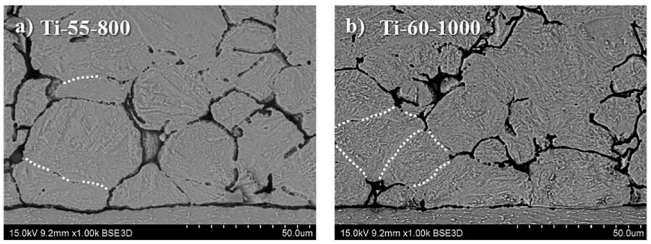

Fig. 8. SEM micrographs of cross sectional cuts of a) Ti-55-800 and b) Ti-60-1000 samples. The samples were etched with Kroll's reagent.

samples showed that the increase in gas temperature and pressure led to denser samples. Moreover, Zhou et al. [42] have experimentally proven that titanium coatings with lower porosities are obtained when spraying with higher process gas temperatures because the interfacial bonding is improved. Conversely, the effect of these process gas parameters on the formation of denser samples has been extensively explained based on the effect of the process gas temperature and pressure on increasing the spraying velocities of the particles, and thus their plastic deformation on the impact [10], [43]. Ultimately, a higher degree of plastic deformation of the particles generally improves sample compaction, reduces porosity, and generates harder samples due to the cold work effect during deformation. In this work, increasing the process gas temperature from 800 to 1000 °C and the pressure from 55 to 60 bar resulted in a 30 % decrease in porosity. Comparing these porosity values with previous studies, the sample sprayed at 1000 °C and 60 bar exhibited similar porosity values to those reported for a CS pure Ti coating sprayed at 1000 °C and 50 bar by Khun et al. [44], which ranged between 4.6 % and 8.2 %. Additionally, the same non-homogeneous porosity distribution along the sample thickness was observed by Khun et al. [44], who also analyzed porosity in three different sections. Conversely, some studies have reported lower porosity coatings for lower process gas temperatures and pressures than those used in the present work. Ajaja et al. [17] and Goldbaum et al. [18] both reported porosity values lower than 3 % and a thickness of 2 mm in CS pure Ti coatings sprayed at 800 °C and 40 bar. This outcome indicates that other parameters in the CS process can affect sample development.

3.2. Mechanical properties

The E and H of the samples showed similar values in both the longitudinal and transverse cross-sectional cuts, as shown in Table 2. This result indicates that there was no anisotropy due to the spraying process.

The E of the CS samples was similar to that of the feedstock powder and consistent with the reported values in the literature for Ti Grade 2 (105-110 GPa [6]). Conversely, the average H value increased by 38 % and 71 % in the Ti-55-800 and Ti-60-1000 samples, respectively, compared to the feedstock powder H, which was 1.41 GPa. However, the H increase was not significant for the Ti-55-800 sample, considering the measurement dispersion. The H was also shown to be higher compared to the reported H for bulk Ti Grade 2 material (1.5-2.0 GPa [19], [20]). Therefore, it was deduced that the H increase was more significant for the sample sprayed at higher process gas temperature and pressure. This result is characteristic of CS samples due to the fabrication process, which is based on the plastic deformation of particles [10]. The particles undergo work hardening when sprayed onto the substrate, usually resulting in an H increase. Previous studies on CS pure Ti samples also reflect similar results, reporting hardness values between 2 and 3 GPa [13], [17].

3.3. Scratch resistance

Fig. 9 shows SEM images of the wear grooves formed on the CS samples by the scratch tests performed at a local scale. The microscopy analysis revealed that the grooves on both samples exhibited similar features. All the grooves showed inhomogeneous pile-up (as observed in Fig. 9a and b), which is a feature associated to plastic deformation by ploughing [45]. Moreover, it was observed that there was a material

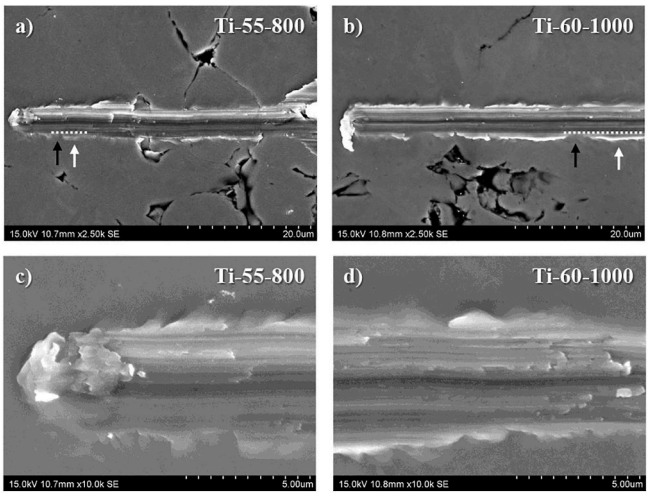

Fig. 9. SEM images showing the wear scar left on the Ti-55-800 (a and c), Ti-60-1000 (b and d) samples after the scratch tests. The upper images correspond to the end of the groove, while the ones below correspond to higher magnification images to highlight the abrasion grooves within the scratch.

chip at the end of the grooves (Fig. 9b and c), what is characteristic of plastic deformation by wedge formation. Regarding the pile-ups, there are regions with no pile-up (indicated by black arrows in the figures) and others with material accumulation at the groove edge (indicated by white arrows, with the groove edge marked by a dotted line). This indicates that the pile-ups generated at each point were not solely a consequence of the ploughed material at that specific point, as material accumulation could also result from ploughed material from previous positions (wedge formation). Additionally, the transverse profiles in Fig. 10 also indicate pile-up development during the scratch tests. These profiles correspond to a scratch test performed on the Ti-60-1000 sample at different positions along the scratch groove, reflecting the non-homogeneity of the pile-up morphology and height. The presence of pile-up confirms the assumption that titanium behaves as a ductile

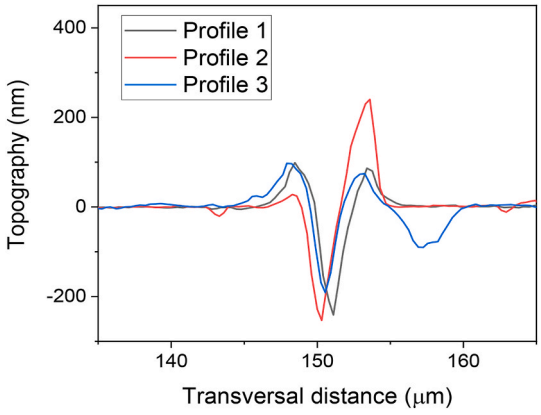

Fig. 10. Transversal profiles corresponding to a scratch test performed on the Ti-60-1000 sample showing the pile-up morphology.

Table 2
E and H values of the Ti-55-800 and Ti-60-1000 samples and the Ti feedstock powder used for spraying.

Material	Elastic modulus, E (GPa)		True hardness, H (GPa)	
	Transversal cross section	Longitudinal cross section	Transversal cross section	Longitudinal cross section
Ti-55–800	116 ± 6	115 ± 5	1.96 ± 0.51	1.94 ± 0.64
Ti-60–1000	110 ± 5	108 ± 4	2.37 ± 0.29	2.41 ± 0.24
Powder	117 ± 3	-	1.41 ± 0.52	-

material, with plastic deformation being the dominant wear mechanism [45]. Furthermore, the grooves exhibited abrasion scratches within them (Fig. 9c and d).

The COF study revealed that its value remained constant during the scratch test when there was low porosity along the scratch line. Fig. 11 shows representative graphs of the COF evolution along the scratch distance for the Ti-55-800 sample. The COF graphs correspond to a test performed along a line with low porosity and another along a line with pores. It can be observed that the COF was variable when pores were present, while it remained constant when there were no pores. This result indicates that the wear mechanisms during the scratch were stable in the absence of microdefects, such as porosity. Moreover, the COF variability was associated with the effect of discontinuities and pores, but not with variations in wear processes. The mean COF values for the Ti-55-800 and Ti-60-1000 samples were estimated to be 0.40 ± 0.07 and 0.31 ± 0.04, respectively.

To use the Archard equation to evaluate the specific wear rate, k_s, the volume of material removed by wear was measured. The wear volume, w, is typically calculated by measuring the weight loss of the sample after the test or by quantifying the residual volume of the groove left in the sample. In a micro-scratch test, it is not possible to measure the weight loss because the amount of worn material is too small to be detected with a balance. Instead, the residual groove volume left by the indenter can be estimated through optical measurements. However, as in this work, when the main wear mechanism is plastic deformation, it must be considered that this residual volume results from both the detached worn material and the material ploughed to the sides or front of the indenter. Therefore, to calculate w, the displaced material per unit distance of the residual groove (v) was first estimated using a confocal microscope, as described in the methods section (Section 2.4). The results show that v was similar in both CS samples (Table 3).

To separate the detached material from that displaced to the sides or front of the indenter, the f_{ab} parameter described by Zum Ghar [46] can be used. This parameter considers the volumes of the residual groove (v) and the pile-ups (v_p) from a cross profile. However, this parameter is only suitable for situations where the pile-up is homogeneous, meaning the material constituting the pile-up at each point is a result of the displaced material from the immediately preceding position. Alternatively, when the pile-up is not homogeneous, the material at each point may consist of displaced material from the immediately preceding position plus accumulated material from earlier points, carried forward by the indenter. Therefore, f_{ab} was calculated using Equation (1), with v and v_p calculated from a groove portion, rather than using the areas of a single cross profile. The estimated volumes (v and v_p), as well as the f_{ab} parameters, are reported in Table 3. The f_{ab} was slightly higher in the Ti-55-800 sample, but the difference was not significant. This implies that the contributions of ploughing and cutting to the material displacement process are similar for both samples. When this parameter is closer to 1, this means that the cutting action prevails, while the ploughing action prevails when the f_{ab} parameter is closer to 0. For the studied materials, it has been seen that the f_{ab} is around 0.4, what indicates that the ploughing process is slightly more dominant than the cutting one. That is, when a hard particle scratches the surface of these samples, their ductile nature tends to deform their surfaces, while reducing the detachment of material.

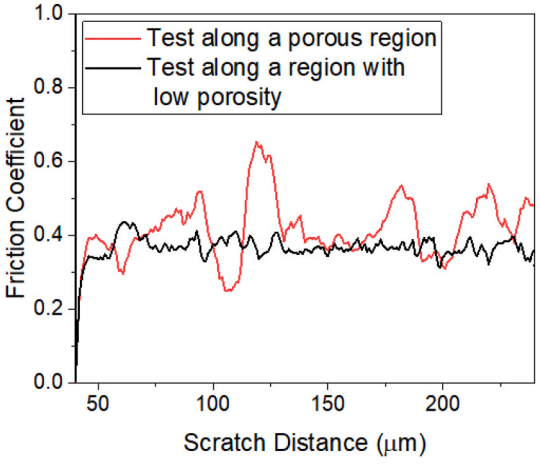

Fig. 11. Representative graphs of the COF evolution with the scratch distance for a test performed along a low porosity region and another one along a region with pores. The tests were performed on the Ti-55-800 sample.

Table 3
Results of the displaced wear volume by the indenter per unit distance (v), the pile-up volume per unit distance (v_p), the f_{ab} parameter, the removed material volume per unit distance (w) and the wear rate (k_s).

Material	v (mm^3/m)	v_p (mm^3/m)	f_{ab}	w (mm^3/m)	k_s (mm^3/Nm)
Ti-800	(6.08 ± 1.49)·10^{-4}	(3.55 ± 0.78)·10^{-4}	0.42 ± 0.16	(2.53 ± 0.62)·10^{-4}	(8.4 ± 2.1)·10^{-3}
Ti-1000	(5.61 ± 1.07)·10^{-4}	(3.46 ± 1.30)·10^{-4}	0.38 ± 0.24	(2.15 ± 0.41)·10^{-4}	(7.2 ± 1.4)·10^{-3}

$$f_{ab} = (v - v_p) / v \quad \text{(Equation 1)}$$

Therefore, the k_s values were obtained using w, estimated as the product of the f_{ab} parameter and v (Table 3). The results indicate that the Ti-55-800 sample exhibited a higher k_s than the Ti-60-1000 sample, although the mean values are not significantly different when considering the error. It should be mentioned that the non-zero value of the removed material volume indicates that there was material removal during the test, and thus, plastic deformation also occurred by the cutting mode, in which material is detached from the surface.

Therefore, the microscopy analysis along with the wear removed volume evaluation has shown that the three wear processes of plastic deformation occurred simultaneously during the scratch experiment. These wear processes are: ploughing (when material is displaced to the sides of the indenter without removal), cutting (when material is detached from the surface), and wedge formation (a form of ploughing at the front, where a fraction of the ploughed material remains on the surface, and another is detached) [45].

The scratch test study has allowed for the intrinsic analysis of the wear performance of the materials, although some microstructural features, like porosity, should be considered. The complexity that the presence of pores generates derives from the fact that the pores result in discontinuities along the scratch path. This implies that there are gaps of material along the scratch where the ploughing action is interrupted. In essence, there is an edge effect when the indenter finds a pore along its path. The importance of microstructural features, such as porosity, on scratch resistance has been previously highlighted by Pitchuka et al. [47] in their work on the scratch evaluation of Al amorphous CS coatings. Scratch tests were performed at different scales, with scratch distances of 0.01 mm or 2 mm, so that the scratches crossed either one splat or several splats, respectively. The analysis of the scratch test results at different scales revealed that the wear rates of longer scratches were dominated by the coatings' microstructural defects. Therefore, the scratch results from the longer scratches did not accurately reflect the wear properties of the material itself. In the present work, the scratch tests have enabled the evaluation of the material's intrinsic response by discarding the data affected by porosity along the scratch length. Furthermore, these tests provide an evaluation of the abrasive action without the influence of other features, such as mechanical mixed layers or oxidation, which typically arise in macroscopic wear tests.

There is limited literature on the evaluation of the scratch resistance of CS Ti samples. However, a previous study by the authors examined the scratch wear on CS Ti6Al4V samples [48], [49], and the results were

found to be comparable to those obtained for the CS pure Ti samples studied here. The CS Ti6Al4V samples were sprayed at process gas temperatures and pressures of 800 °C and 40 bar, and 1100 °C and 50 bar, respectively [48], [49]. The 800 °C sample exhibited 79 % higher porosity than the 1100 °C sample, and the k_s was an order of magnitude higher. These differences may be attributed to the varying porosities and thus do not reflect the material's intrinsic response. This highlights the capabilities of the wear rate study discounting the pores, as done in this work, which allows for a comparison of the material properties unaffected by defects like porosity.

3.4. Wear behavior under reciprocating conditions

The study of the material's intrinsic behavior is important, as described in the previous section. However, its behavior in service is also essential. Understanding its response on a macroscopic scale, where defects contribute to its behavior, allows us to determine whether the material is suitable for its real-world application. Table 4 shows the total number of cycles at which the wear limit condition of 1 mm pin height loss was reached for each material and oscillation angle. It was observed that the Ti-55-800 sample reached the limit condition after a lower number of cycles than the Ti-60-1000 sample, except for the 30° angle. This table also provides the total sliding distance accumulated under each testing condition up to the point at which the 1 mm pin height reduction was reached. It can be observed that the sliding distance decreases dramatically for the 120° angle.

The macroscopic wear rates of the CSAM samples, evaluated from weight loss measurements, are reported in Fig. 12a. The results of the experiments performed at 30° and 60° oscillation angles are similar for both materials, showing values between $1.5{\cdot}10^{-4}$ and $1.9{\cdot}10^{-4}$ mm^3/Nm. However, both materials also showed an increase in wear rate during the tests performed at an angle of 120°. The wear rates in the 120° angle experiments were $(6.8 \pm 1.7){\cdot}10^{-4}$ mm^3/Nm for the Ti-55-800 sample and $(3.8 \pm 1.6){\cdot}10^{-4}$ mm^3/Nm for the Ti-60-1000 sample. The variability observed in the wear rate values, as indicated by the corresponding standard deviations, is a consequence of the characteristic microstructure of these coatings, formed by the bonding of splats resulting from particle impacts with different deformation gradients. These deviations are smaller at angles of 30° and 60° and fall within an acceptable range. However, it considerably increased at 120° (Fig. 12a). This increase may be due to highly aggressive conditions for this type of CSAM sample. Nevertheless, it should be noted that this amplitude represents a limiting test condition.

Regarding the COF measurements, Fig. 12b presents the mean values calculated from the stable regime of each test. The evolution of the coefficient of friction during the tests was characterized by an initial transient regime prior to reaching the steady state. This transient regime occurred during the first cycles. Therefore, for the calculation of the COF, the values corresponding to the first 10% of the cycles were discarded, and the average value was obtained from the remaining 90%. The results show that, for both materials, the COF was obtained in the tests performed applying 30° and 60° oscillation angles was 0.55-0.6, while for the tests performed at 120°, the COF was ~ 0.43. Comparing the results shown in Fig. 12a and b, it can be seen that the wear rate was higher for the 120° angle despite showing a lower coefficient of friction.

Table 4
Number of cycles and total sliding distance of the reciprocating wear tests.

Material	Angle (°)	Number of cycles ($\cdot 10^4$)	Total sliding distance (m)
Ti-800	30	2.85	775
	60	1.24	673
	120	0.20	218
Ti-1000	30	2.64	720
	60	1.65	896
	120	0.35	386

These results pointed out that different wear mechanisms were occurring in the tests performed with the highest sliding amplitude.

In the oscillatory setup, increasing the oscillation angle to 120° inherently increases both the arc length per cycle and the sliding speed. A higher sliding speed raises the instantaneous frictional power and the flash temperature at the contact, which may trigger transitions in the severity and the wear mechanism (e.g., from mild abrasion/adhesion to adhesive-severe or oxidative regimes), thereby increasing the wear rate, although the average coefficient of friction remained nearly unchanged. Although the COF at 120° was lower (~0.43) compared to 30°–60° (0.55–0.60), the sliding speed doubled with respect to 60° and quadrupled relative to 30°. Because, the energy dissipated per unit time, evaluated through the frictional power, increased from ~1.11 W (30°) to ~2.43 W (60°) and ~3.48 W (120°), despite the lower COF (Table 5). That is, at 120°, the friction power triples compared to that developed during the tests at 30° and turns out to be 1.5 times higher than that obtained for 60°. This higher frictional power may explain the higher wear rate at 120°, promoting the transitions to severe wear. The combination of higher speed and greater sliding distance per cycle (and per minute) increased the cumulative mechanical and thermal load on the pin, thereby accelerating wear even under a slightly lower friction coefficient.

The wear mechanisms were therefore analyzed conducting a SEM investigation on the plane and transversal view of the surface of the worn samples (Figs. 13–15). The plane view images of the samples' surfaces (Fig. 13) displayed various features related to the wear process. In these images, which were acquired using the BSE detector, the areas with the darkest contrast, such as the one indicated in Fig. 13a, correspond to oxidized particles in the MML. The oxidation is caused due to the temperature increase from the reciprocating motion in the contact. Additionally, these images show that counterface particles were also observed trapped on the sample surface (the lightest contrasted areas), as indicated in Fig. 13b. The mechanical action in the contact also generated abrasive grooves and cracks (an example is pointed out in Fig. 13d), which are characteristic of sliding wear processes dominated by plastic deformation and fatigue. It should be noted that all the observed features were present in both samples and under all testing conditions.

The transversal view study of the worn samples is presented in Fig. 14. These images revealed the presence of the MML on the top surface, as well as cracks oriented parallel to the surface, which are highlighted by dashed lines in the images. Regarding the MMLs, the images indicate that oxidized particles were trapped at the surface, with a higher extent in the tests conducted at oscillating angles of 30° and 60° (Fig. 14a, b, d and e).

The oxide composition of the MMLs was similar for all the tested samples. Fig. 15 presents the analysis of the MML's chemical composition of the samples tested at 30° and 120° for both studied materials. It can be seen that the MML consisted of a mixture of small particles formed due to the mechanical milling associated with MML formation during the test. The particles appeared less compacted at the top surface. The EDX analyses performed on particles with different chemical compositions indicate that the MML consisted of a mixture of Ti and steel particles with oxidation. As a reference, EDX 1 in all the samples corresponds to the chemical composition of the Ti sample. Concerning the cracks, they were generated parallel to the surface, what is a distinctive feature of delamination wear derived from the fatigue wear caused by the reciprocating movement [50].

Additionally, the microscopy analysis revealed material delamination at the pins' sides, as illustrated in Fig. 16. This outcome was more pronounced in the tests performed at 120°, and in the ones performed on the Ti-55-800 material. The delamination effect was also observed in the acquired measurement of the linear displacement of the pin due to the removed wear volume at the pins' surface, which is presented in Fig. 17. Oscillations in the linear displacement were observed, indicating transitions in the wear behavior. These changes correspond to the onset of

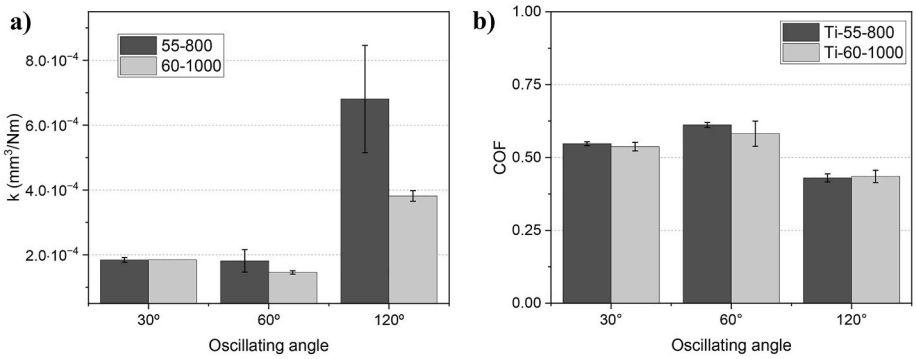

Fig. 12. Specific wear rates (k) and coefficient of friction (COF) of the samples tested under reciprocating conditions at three different oscillation angles (30°, 60° and 120°).

Table 5
Sliding kinematics, normal load and frictional power for the different oscillation angles.

Angle (°)	Speed, v (mm/s)	COF, μ	Normal load, W (N)	Frictional power, P = μ·W·v (W)
30	24.5	0.55	82.5	1.112
60	49	0.6	82.5	2.425
120	98	0.43	82.5	3.477

delamination processes at particular cycle intervals during the experiments, as confirmed by the surface damage characteristics displayed in Figs. 13, 14 and 16.

Therefore, it was concluded that delamination was the dominant wear process, followed by oxidation. Delamination and oxidation were particularly present in the tests performed at 30° and 60°. In contrast, in the tests performed at 120°, oxidation was less important, and the delamination wear process was severe. The increased severity of delamination was related to the more aggressive testing conditions [51], as the increase in the oscillation angle resulted in higher sliding velocities. It should be noted that the observed difference in wear mechanisms in the tests performed at the highest oscillation angle was accompanied by a COF reduction, as reported in Fig. 12. Furthermore, the observed higher delamination in the Ti-55-800 samples was related to the higher porosity of this sample. Increased porosity implies that the splats have a lower degree of bonding between them, facilitating their detachment. Therefore, although the metallurgical bonding of splats in Ti samples is strong enough to build up a thick sample with a low number of created links between the sprayed particles, the splats present a weaker attachment. This outcome was also reflected in the work by Goldbaum

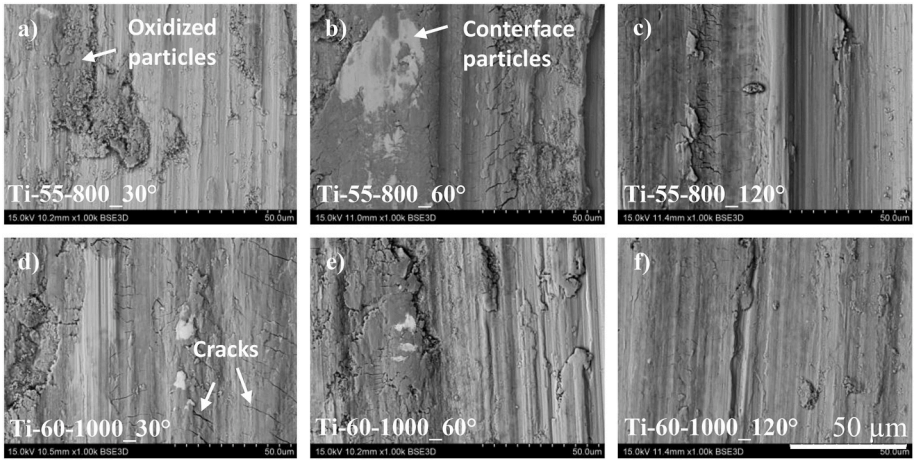

Fig. 13. SEM-BSE images of plane view surfaces corresponding to the Ti-55-800 (a, b and c) and Ti-60-1000 (d, e and f) worn samples tested under reciprocating sliding with oscillation angles of 30°, 60° and 120°.

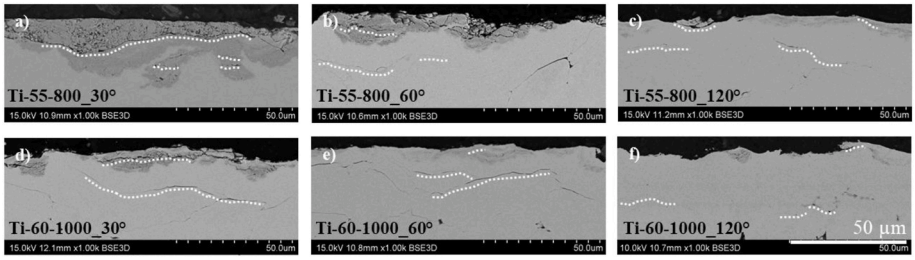

Fig. 14. SEM-BSE images of transversal view sections corresponding to the Ti-55-800 (a, b and c) and Ti-60-1000 (d, e and f) worn samples tested under reciprocating sliding with oscillation angles of 30°, 60° and 120°. The dashed lines delineate fatigue cracks parallel to the surface.

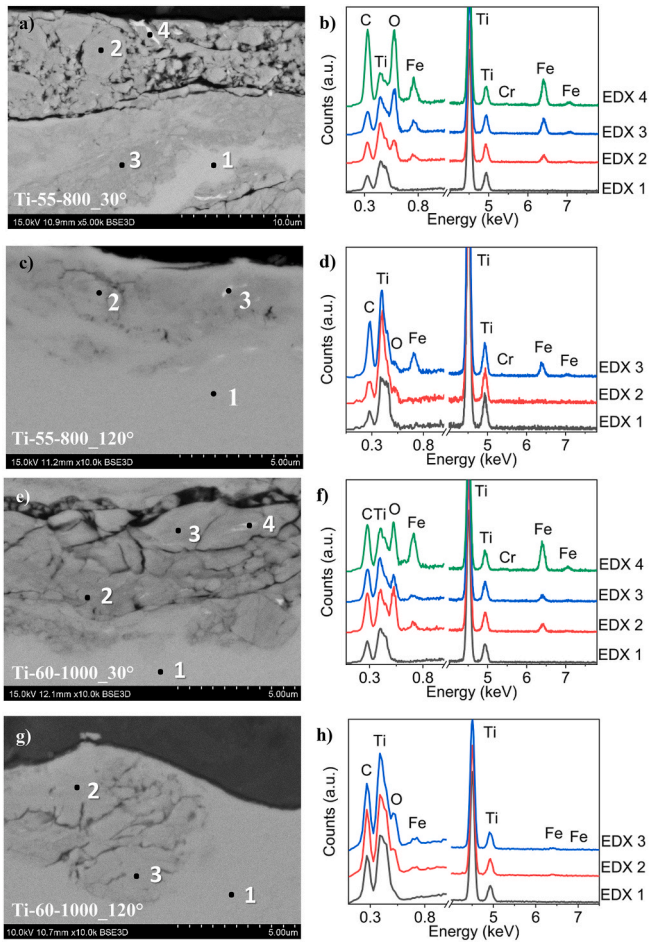

Fig. 15. SEM-BSE image showing a higher magnification of the MML and the corresponding EDX analysis performed that the sites indicated in the images for the tested samples of Ti-55-800 at oscillation angles of 30° (a,b) and 120° (c,d) and of the tested samples of Ti-60-1000 at oscillation angles of 30° (e,f) and 120° (g, h).

et al. [18] on CS Ti samples. In their work, the porosity and splat adhesion strength were examined in different samples sprayed using various particle velocities. The results show that both sample density and splat adhesion strength increase with increasing particle velocity, indicating a relationship between these characteristics. Moreover, the effect of a weak bonding between the sample particles on favoring delamination wear was reported by Zhou et al. [52]. They performed ring-on-ring sliding friction tests of copper metal matrix composites with different iron volume content and their results showed how delamination was facilitated by the generation and propagation of fatigue cracks at the iron particle boundaries.

These findings have revealed that the Ti-60-1000 sample exhibited better performance in terms of reciprocating wear resistance. This outcome was associated with the lower porosity of this sample, which limited the delamination process during the wear experiment. However, it was observed that the wear rate still increased during the test conducted under the most aggressive condition, at an oscillation angle of 120°. The aggressiveness of this condition is related to the higher sliding velocity combined with the higher arc length. The limitations of this study are related to the inability to determine which wear variable has the most significant effect on the wear rate: the arc length or the sliding velocity. Therefore, future work should consider conducting an experimental plan to identify the most significant effects and interactions of the different variables involved in the system: the sliding velocity, and the arc length and frequency of oscillation. As observed, although the behavior of the material without defects, evaluated on a microscale, is similar, the behavior on a macroscale shows differences that are controlled by the presence of defects and bonding characteristics between the splats. This indicates the necessity of researching towards obtaining a CS-sprayed material free of defects or at least with a controlled percentage of defects.

Moreover, it should be mentioned that the obtained wear rates, in the range of 10^{-4} mm^3/Nm, are high for the application of this material. In order to reduce the wear rate, the sample structure should be improved by modifying the processing parameters or applying a heat treatment after deposition. Moreover, lubricated conditions should be evaluated, as they are closer to the actual applications and they are expected to reduce significantly the wear rate. However, the obtained wear rates were in the order of magnitude of those obtained for CS pure Ti samples in different wear configurations. For example, Khun et al. [22] reported wear rates from $1.1{\cdot}10^{-4}$ to $2.2{\cdot}10^{-4}$ mm^3/Nm from rotational ball-on-disc experiments using a 100Cr6 steel ball in dry conditions. Another example is the work performed by Alidokht et al. [23], where they report a wear rate of $9.5{\cdot}10^{-4}$ mm^3/Nm from reciprocating ball-on-flat experiments without lubricant and using an alumina ball.

Thus, regarding the potential application of this material for components subjected to reciprocating sliding wear, further investigation is needed considering the improvement of the sample density as well as performing a more extensive wear experimental plan. The extended experimental plan should also consider specifying a particular application to better adapt the testing conditions to the real environment and the use of corresponding lubricants. Additionally, reducing sample porosity by tuning the CS process parameters should be considered. On the other hand, if Ti is used for the structural parts, this preliminary analysis suggests that both samples, Ti-50-800 and Ti-60-1000, could be suitable. The mechanical properties of the components were evaluated in this work at the local scale, and the results showed similar values to those of the bulk material. However, future work should also evaluate the mechanical properties at the macroscale, as these properties are also affected by the presence of porosity and defects.

4. Conclusions

This study investigated the applicability of the CSAM technique to manufacture pure Ti (Grade 2) components which are subjected to reciprocating wear conditions. Two Ti CSAM samples sets were fabricated using different process parameters. The varied spraying parameters were the process gas temperature and pressure, defined for each sample as follows: 55 bar and 800 °C (Ti-55-800 sample) and 60 bar and

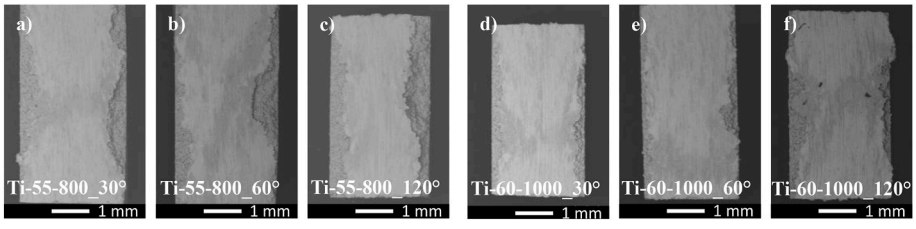

Fig. 16. SEM-BSE images of the worn surfaces after the reciprocating wear tests in the Ti-55-800 (a, b and c) and the Ti-60-1000 (d, e and f) samples.

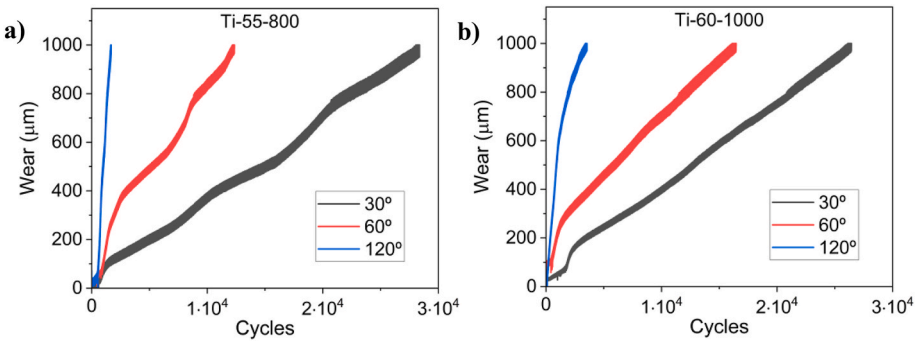

Fig. 17. Linear displacement of the pin during the reciprocating wear tests performed on the a) Ti-55-800 and the b) Ti-60-1000 samples.

1000 °C (Ti-60-1000 sample). The samples were evaluated through microstructural analysis, mechanical and tribological properties at the local scale, and macroscopic tribological behavior under reciprocating sliding conditions to simulate back-and-forth motions of materials in contact.

The results have shown that the different processing parameters led to samples with varying levels of porosity. The Ti-60-1000 sample's microstructure was characterized by a lower porosity degree, approximately 30 % lower than that of the Ti-55-800 sample. Regarding the mechanical characterization, it was shown that the hardness was increased by a 38 % and a 71 % in the Ti-55-800 and Ti-60-1000 samples, respectively, compared to the feedstock powder H.

The scratch wear evaluation at the local scale revealed that the samples presented similar wear resistances. Moreover, they were both worn by plastic deformation through ploughing, cutting and wedge formation processes, as evidenced by the developed pile-up and abrasive grooves. The wear process was shown to be stable, as deduced from the constant value of the coefficient of friction (COF) along the scratch distance. The f_{ab}parameter allowed for the determination of the wear rate of material removal from the surface. The determined wear rates were $(8.4 \pm 2.1)\cdot10^{-3}$ and $(7.2 \pm 1.4)\cdot10^{-3}$ mm^3/Nm for the Ti-55-800 and Ti-60-1000 samples, respectively.

Regarding the tribological behavior at the macroscopic scale, the Ti-60-1000 sample exhibited higher wear resistance under the reciprocating sliding conditions studied in this work. In the experiments performed at 30° and 60° oscillating angles similar wear rates were obtained for both materials, showing values between $1.5\cdot10^{-4}$ and $1.9\cdot10^{-4}$ mm^3/Nm. However, both materials also showed an increase in wear rate during the tests performed at an angle of 120°. The wear rates in the 120° oscillation angle experiments were $(6.8 \pm 1.7)\cdot10^{-4}$ mm^3/Nm for the Ti-55-800 sample and $(3.8 \pm 1.6)\cdot10^{-4}$ mm^3/Nm for the Ti-60-1000 sample. The obtained COF were similar for both studied samples, showing values around 0.55 in the tests at 30° and 60° oscillation angles, and around 0.43 for the tests at 120°. The reduction in wear rate at high sliding amplitudes compared to the Ti-55-800 sample was attributed to the weaker attachment between the splats in the Ti-55-800 sample, which intensified the delamination during the tests. Furthermore, the evaluation of wear mechanisms revealed that both samples exhibited the same wear mechanisms, oxidation and delamination, although at the highest test oscillation angle the delamination process was more severe.

Although the present study is preliminary, the results indicate that manufacturing Ti parts using the CSAM technology shows promising potential for application for structural Ti components. These positive perspectives are based on the environmental and economic benefits of using the CSAM process. Finally, the application of components manufactured by CSAM requires further research focused on reducing porosity and increasing the bonded areas at the splat contours.

CRediT authorship contribution statement

Paloma Sirvent: Writing – original draft, Visualization, Investigation, Formal analysis. **Xavier Soldani:** Methodology, Investigation, Formal analysis. **Miguel Ángel Garrido-Maneiro:** Writing – review & editing, Project administration, Methodology, Conceptualization. **Pedro Poza:** Writing – review & editing, Project administration, Methodology, Conceptualization.

Declaration of generative AI and AI-assisted technologies in the writing process

During the preparation of this work the authors used an IA assistant in order to revise the language. After using this tool, the authors reviewed and edited the content as needed and take full responsibility for the content of the publication.

Declaration of competing interest

The authors declare that they have no known competing financial interests or personal relationships that could have appeared to influence the work reported in this paper.

Acknowledgements

The authors wish to acknowledge the financial support received from the Spanish government AEI under Grants No. PID2020-115508RB-C22 (A3M) and PID2023-146720OB-C21 (HEA4COAT).

Data availability

Data will be made available on request.

References

[1] K.M. Rajan, A.K. Sahoo, B.C. Routara, A. Panda, R. Kumar, A review on various approaches of 3D printing of Ti-Alloy, Mater. Today Proc. 62 (2022) 3865–3868, https://doi.org/10.1016/j.matpr.2022.04.532.
[2] H.D. Nguyen, et al., A critical review on additive manufacturing of Ti-6Al-4V alloy: microstructure and mechanical properties, J. Mater. Res. Technol. 18 (2022) 4641–4661, https://doi.org/10.1016/j.jmrt.2022.04.055.
[3] S. Liu, Y.C. Shin, Additive manufacturing of Ti6Al4V alloy: a review, Mater. Des. 164 (2019) 107552, https://doi.org/10.1016/j.matdes.2018.107552.
[4] A. Mouritz, Introduction to Aerospace Materials, first ed., Woodhead Publishing, Cambridge, 2012.
[5] M. Merola, S. Affatato, Materials for hip prostheses: a review of wear and loading considerations, Materials 12 (3) (2019), https://doi.org/10.3390/ma12030495.
[6] C. Leyens, M. Peters (Eds.), Titanium an Titanium Alloys, Wiley-VCH Verlag, 2003, https://doi.org/10.1002/3527602119.
[7] M. Peters, J. Kumpfert, C.H. Ward, C. Leyens, Titanium alloys for aerospace applications, Adv. Eng. Mater. 5 (6) (2003) 419–427, https://doi.org/10.1002/adem.200310095.
[8] S.S. Maurya, N. Kumari, A.K. Grain, A.K. Keshri, High-temperature tribological performance of nanodiamond-reinforced titanium coatings fabricated via shrouded

plasma spray, Mater. Today Commun. 49 (2025) 113923, https://doi.org/10.1016/j.mtcomm.2025.113923.
[9] S. Singh, N. Kumar, T. Chowdhury, V. Sharma, Microstructural and electrochemical evaluation of Cu-TiO2 composite coatings fabricated by cold spray, HVOF, and flame spray, Ceram. Int. (2026), https://doi.org/10.1016/j.ceramint.2026.01.454.
[10] J. Villafuerte (Ed.), Modern Cold Spray: Materials, Process, and Applications, first ed., Springer, 2015 https://doi.org/10.1007/978-3-319-16772-5.
[11] P. Poza, M.Á. Garrido-Maneiro, Cold-sprayed coatings: microstructure, mechanical properties, and wear behaviour, Prog. Mater. Sci. 123 (June 2021) (2022), https://doi.org/10.1016/j.pmatsci.2021.100839.
[12] Y. Zou, Cold spray additive manufacturing: microstructure evolution and bonding features, Acc. Mater. Res. 2 (11) (2021) 1071–1081, https://doi.org/10.1021/accountsmr.1c00138.
[13] P. Sirvent, et al., Surface topography analysis in cold spray additive manufacturing, Precis. Eng. 92 (July 2024) (2025) 207–218, https://doi.org/10.1016/j.precisioneng.2024.12.007.
[14] F.N. Lomo, A. Vargas-Uscategui, P.C. King, M.J. Patel, I.S. Cole, Microstructure and mechanical properties of heat-treated cold spray additively manufactured titanium metal matrix composites, J. Manuf. Process. 99 (February) (2023) 12–26, https://doi.org/10.1016/j.jmapro.2023.04.077.
[15] G. Bae, et al., Bonding features and associated mechanisms in kinetic sprayed titanium coatings, Acta Mater. 57 (19) (2009) 5654–5666, https://doi.org/10.1016/j.actamat.2009.07.061.
[16] W. Wong, E. Irissou, A.N. Ryabinin, J.G. Legoux, S. Yue, Influence of helium and nitrogen gases on the properties of cold gas dynamic sprayed pure titanium coatings, J. Therm. Spray Technol. 20 (1–2) (2011) 213–226, https://doi.org/10.1007/s11666-010-9568-y.
[17] J. Ajaja, D. Goldbaum, R.R. Chromik, Characterization of Ti cold spray coatings by indentation methods, Acta Astronaut. 69 (2011) 923–928, https://doi.org/10.1016/j.actaastro.2011.06.012.
[18] D. Goldbaum, et al., Mechanical behavior of Ti cold spray coatings determined by a multi-scale indentation method, Mater. Sci. Eng. A 530 (2011) 253–265, https://doi.org/10.1016/j.msea.2011.09.083.
[19] H.S. Lim, M.J. Hwang, H.N. Jeong, W.Y. Lee, H.J. Song, Y.J. Park, Evaluation of surface mechanical properties and grindability of binary Ti alloys containing 5 wt % Al, Cr, Sn, and V, Metals 7 (11) (2017) 1–11, https://doi.org/10.3390/met7110487.
[20] C.M.F.A. Cossú, et al., Mechanical and microstructural characterization of AS-CAST Ti-12Mo-xNb alloys for orthopedic application, Mater. Res. 22 (Suppl 1) (2019) 1–5, https://doi.org/10.1590/1980-5373-MR-2019-0178.
[21] Y. Zhu, L. Song, Z. Deng, L. Zhao, J. He, Study of the friction and wear behavior of Ti-6Al-4V alloy under low temperatures, JOM 77 (3) (2025) 1659–1670, https://doi.org/10.1007/s11837-024-07105-0.
[22] N.W. Khun, A.W.Y. Tan, E. Liu, Mechanical and tribological properties of cold-sprayed Ti coatings on Ti-6Al-4V substrates, J. Therm. Spray Technol. 25 (4) (2016) 715–724, https://doi.org/10.1007/s11666-016-0396-6.
[23] S.A. Alidokht, V.N.V. Munagala, R.R. Chromik, Role of third bodies in friction and wear of cold-sprayed Ti and Ti–TiC composite coatings, Tribol. Lett. 65 (3) (2017) 1–15, https://doi.org/10.1007/s11249-017-0899-4.
[24] R.F. Váz, et al., Fretting wear and scratch resistance of cold - sprayed pure Cu and Ti, Metallogr. Microstruct. Anal. 10 (4) (2021) 496–513, https://doi.org/10.1007/s13632-021-00758-2.
[25] P. Sirvent, M.A. Garrido, S. Lozano-Perez, P. Poza, Oscillating and unidirectional sliding wear behaviour of cold sprayed Ti-6Al-4V coating on Ti-6Al-4V substrate, Surf. Coating. Technol. 382 (Jan. 2020) 125152, https://doi.org/10.1016/j.surfcoat.2019.125152.
[26] R. Kyle Schmidt, The Design of Aircraft Landing Gear, SAE International, 2020.
[27] B. Sagbas, Biotribology of artificial hip joints, in: P.H. Darji (Ed.), Advances in Tribology, IntechOpen, Rijeka, 2016, https://doi.org/10.5772/64488.
[28] M. Fellah, M. Labaiz, O. Assala, L. Dekhil, A. Iost, Tribological behavior of biomaterials for total hip prosthesis, Trends Biomater. Artif. Organs 29 (1) (2015) 22–30.
[29] N.R. Rundora, D.E.P. Klenam, S. Polat, N.M. Mathabathe, J. van der Merwe, M. O. Bodunrin, Dry sliding wear behavior of experimental low-cost titanium alloys, Tribol. Trans. 67 (3) (2024) 560–572, https://doi.org/10.1080/10402004.2024.2357288.
[30] W. Wong, P. Vo, E. Irissou, A.N. Ryabinin, J.G. Legoux, S. Yue, Effect of particle morphology and size distribution on cold-sprayed pure titanium coatings, J. Therm. Spray Technol. 22 (7) (2013) 1140–1153, https://doi.org/10.1007/s11666-013-9951-6.
[31] M.F. Morks, S.H. Zahiri, X.B. Chen, S. Gulizia, A. Vargas-Uscategui, I.S. Cole, Influence of gas temperature and heat treatment on microstructure and properties of cold sprayed commercially pure titanium, J. Mater. Eng. Perform. 31 (7) (2022) 5549–5558, https://doi.org/10.1007/s11665-022-06621-x.
[32] K. Binder, J. Gottschalk, M. Kollenda, F. Gärtner, T. Klassen, Influence of impact angle and gas temperature on mechanical properties of titanium cold spray deposits, J. Therm. Spray Technol. 20 (1–2) (2011) 234–242, https://doi.org/10.1007/s11666-010-9557-1.
[33] P. Sirvent, M.A. Garrido, C.J. Múnez, P. Poza, S. Vezzù, Effect of higher deposition temperatures on the microstructure and mechanical properties of Al 2024 cold sprayed coatings, Surf. Coating. Technol. 337 (2018), https://doi.org/10.1016/j.surfcoat.2018.01.055.
[34] M.A. Garrido, P. Sirvent, P. Poza, Evaluation of mechanical properties of Ti6Al4V cold sprayed coatings, Surf. Eng. 34 (5) (2017) 399–405, https://doi.org/10.1080/02670844.2017.1398442.
[35] W.C. Oliver, G.M. Pharr, Measurement of hardness and elastic modulus by instrumented indentation: advances in understanding and refinements to methodology, J. Mater. Res. 19 (1) (2004) 3–20, https://doi.org/10.1557/jmr.2004.19.1.3.
[36] D. Merino-Millan, M.Á. Garrido-Maneiro, C.J. Múnez, P. Poza, Hardness and Young's modulus evolution of low-power plasma sprayed inconel 625 coatings exposed to high temperatures, Surf. Coating. Technol. 494 (July) (2024), https://doi.org/10.1016/j.surfcoat.2024.131527.
[37] W.D. Nix, H. Gao, Indentation size effects in crystalline materials: a law for strain gradient plasticity, J. Mech. Phys. Solid. 46 (3) (Mar. 1998) 411–425, https://doi.org/10.1016/S0022-5096(97)00086-0.
[38] I. Hutchings, P. Shipway, Tribology: Friction and Wear of Engineering Materials, second ed., Elsevier Ltd, Oxford, 2017.
[39] J.F. Archard, Contact and rubbing of flat surfaces, J. Appl. Phys. 24 (981) (1953).
[40] N.S. Karmarkar, V. V Varadaraajan, P.S. Mohanty, S.K. Nagendiran, An attempt to understand stainless 316 powders for cold-spray deposition, Powders 2 (1) (2023) 151–168, https://doi.org/10.3390/powders2010011.
[41] S. Gulizia, et al., Microstructure and mechanical properties of cold spray titanium coatings, in: Thermal Spray: Global Solutions for Future Application, 2010, pp. 95–98.
[42] H.X. Zhou, Z.J. Li, S.W. Jiang, Effect of gas temperature on the interfacial bonding of cold-spray additive-manufactured Ti6Al4V, Surf. Interfaces 44 (October 2023) (2024), https://doi.org/10.1016/j.surfin.2023.103676.
[43] L. Alonso, M.A. Garrido-Maneiro, P. Poza, A study of the parameters affecting the particle velocity in cold-spray: theoretical results and comparison with experimental data, Addit. Manuf. 67 (March) (2023) 103479, https://doi.org/10.1016/j.addma.2023.103479.
[44] N.W. Khun, A.W.Y. Tan, W. Sun, E. Liu, Wear and corrosion resistance of thick Ti-6Al-4V coating deposited on Ti-6Al-4V substrate via high-pressure cold spray, J. Therm. Spray Technol. 26 (2017) 1393–1407, https://doi.org/10.1007/s11666-017-0588-8.
[45] B. Bhushan, Introduction to Tribology, second ed., John Wiley & Sons, Ltd., 2013 https://doi.org/10.1002/9781118403259. The Atrium.
[46] K.H. Zum Gahr, Modelling of two-body abrasive wear, Wear 124 (1988) 87–103.
[47] S.B. Pitchuka, D. Lahiri, G. Sundararajan, A. Agarwal, Scratch-induced deformation behavior of cold-sprayed aluminum amorphous/nanocrystalline coatings at multiple load scales, J. Therm. Spray Technol. 23 (3) (2014) 502–513, https://doi.org/10.1007/s11666-013-0021-x.
[48] M.Á. Garrido, P. Sirvent, D. Elvira, Á. Rico, C.J. Múnez, P. Poza, Response of cold sprayed Ti6Al4V coatings to solid particle erosion and micro-scratch wear processes, Mater. Sci. Forum 941 (Dec. 2018) 1680–1685. https://doi.org/10.4028/www.scientific.net/MSF.941.1680.
[49] P. Sirvent, M.Á. Garrido-Maneiro, P. Poza, Improving cold sprayed Ti-6Al-4V coatings controlling processing parameters: effect on microstructure and scratch behaviour, Wear (May) (2023) 532–533, https://doi.org/10.1016/j.wear.2023.205075.
[50] N.P. Suh, An overview of the delamination theory of wear, Wear 44 (1) (1977) 1–16, https://doi.org/10.1016/0043-1648(77)90081-3.
[51] A. Molinari, G. Straffelini, B. Tesi, T. Bacci, Dry sliding wear mechanisms of the Ti6Al4V alloy, Wear 208 (1–2) (1997) 105–112, https://doi.org/10.1016/S0043-1648(96)07454-6.
[52] H. Zhou, et al., Friction and wear maps of copper metal matrix composites with different iron volume content, Tribol. Int. 132 (September 2018) (2019) 199–210, https://doi.org/10.1016/j.triboint.2018.11.027.